AIP Advances

Large depth of focus plasmonic metalenses based on Fresnel biprism

Cite as: AIP Advances **10**, 045025 (2020); https://doi.org/10.1063/5.0004208
Submitted: 10 February 2020 . Accepted: 30 March 2020 . Published Online: 14 April 2020

Adriana Inclán Ladino, Job Mendoza-Hernández, Maximino Luis Arroyo-Carrasco, Rafael Salas-Montiel, Manuel García-Méndez, Victor Coello, and Ricardo Tellez-Limon

Large depth of focus plasmonic metalenses based on Fresnel biprism

Cite as: AIP Advances 10, 045025 (2020); doi: 10.1063/5.0004208
Submitted: 10 February 2020 • Accepted: 30 March 2020 •
Published Online: 14 April 2020

Adriana Inclán Ladino,[1] Job Mendoza-Hernández,[2] Maximino Luis Arroyo-Carrasco,[3] Rafael Salas-Montiel,[4] Manuel García-Méndez,[1] Victor Coello,[5] and Ricardo Tellez-Limon[6,a)]

AFFILIATIONS

[1]CICFIM-Universidad Autónoma de Nuevo León, Avenida Universidad S/N, San Nicolás de los Garza, Nuevo León 66450, Mexico
[2]Tecnológico de Monterrey, Escuela de Ingeniería y Ciencias, Av. Eugenio Garza Sada 2501, Monterrey, Nuevo León 64849, Mexico
[3]FCFM-Benemérita Universidad Autónoma de Puebla, Av. San Claudio y 18 Sur, Col. San Manuel, Puebla, Puebla 72570, Mexico
[4]Department of Physics, Mechanics, Materials and Nanotechnology, Institut Charles Delaunay / L2n CNRS ERL 7004, Université de Technologie de Troyes, 12 rue Marie Curie CS 42060, 10004, Troyes, France
[5]Unidad Monterrey, Centro de Investigación Científica y de Educación Superior de Ensenada, Alianza Centro 504, PIIT, Apodaca, Nuevo León 66629, Mexico
[6]CONACYT-Unidad Monterrey, Centro de Investigación Científica y de Educación Superior de Ensenada, Alianza Centro 504, PIIT, Apodaca, Nuevo León 66629, Mexico

[a)]**Author to whom correspondence should be addressed:** rtellez@conacyt.mx

ABSTRACT

Plasmonic metalenses are optical elements that are able to shape the amplitude and the phase of light with a high spatial resolution, standing as promising elements for new low-weight imaging technologies. A desired characteristic for metalenses is to have an extended depth of focus (DOF) to bring a larger tolerance of placement of the image plane, reducing image blurring and increasing light directivity. Based on the Fresnel biprism and using the integral equation method, we numerically demonstrate light focusing with cylindrical plasmonic metalenses that are able to generate large DOF values of up to 150λ with transmission efficiencies around 50%. The easiness in the design of our plasmonic metalenses represents an advantage in terms of fabrication, opening new possibilities for the development of small-size lenses for light focusing and imaging applications.

I. INTRODUCTION

Since the demonstration of extraordinary optical transmission through thin metallic films structured with subwavelength hole arrays,[1] new horizons have been opened in the design and fabrication of flat metasurfaces to control light transmission close to the diffraction limit, a situation hardly achievable with bulk-optical systems.[2,3] With these plasmonic metasurfaces, it is possible to control amplitude, phase,[4,5] polarization, and even orbital angular momentum[6,7] to achieve structured light beams.[8–10]

Among the large variety of metasurfaces can be found plasmonic metalenses (PMs), devices that allow light focusing in reduced spatial regions. Their operation principle is based on the constructive interference of light scattered by each one of the subwavelength structures (scatterers) placed in the surface of a thin metallic layer.[11] Hence, their efficiency and design are directly linked to the geometry of the scatterers. Because of their reduced size, these lenses can be applied as flat compact imaging systems for subwavelength focusing and beam shaping.[11–17]

For imaging applications, it is desired that PMs present a large depth of focus (DOF) without losing spatial lateral resolution to reduce alignment requirements.[18] This is a challenging situation because of the small size of these flat metasurfaces. For this purpose, different approaches have been proposed, like PMs formed by

complex arrays of Y-shaped nanoantennas[19] or nanorods,[20] with the reported DOF varying from 64λ to 74λ for this kind of systems.[21] However, due to the spatial variation of these scatterers, it is not intuitive to predict the behavior of these large DOF PMs. Less complex arrays of scatterers have also been proposed for the design of PMs, like multilayered arrays of concentric rings, but only short DOF values have been achieved (3.6λ).[22]

Another option for light focusing is by employing nanoslits practiced in thin metallic layers.[16,17] This kind of metalenses produce cylindrical wavefronts resulting from the constructive interference of light coming out from each nanoslit. The phase of each wavefront can be computed through the dispersion relation of a three-layered medium as a function of its width, thickness of the metallic layer, and lateral position of the nanoslit.[23] To achieve light focusing, it is only necessary to match the phase of these outcoming wavefronts to the phase induced by a classical optical element.[16,17] For the theoretical design of these PMs, different numerical methods, such as FDTD (finite-difference time domain),[12,16] FDFD (finite-difference frequency-domain),[17] or fast Fourier transform algorithms, have been employed.[19] More recently, the use of adjoint optimization-based inverse electromagnetic design has also been proposed for the design of PMs, with DOF values of almost 20λ being demonstrated with efficiencies of up to 24%.[18] While these differential methods bring a good insight into the instantaneous energy flow for near-field characterization, they present inaccuracies in the far-field regime since they require discretization of the scatterers and also the surrounding space,[24] leading to uncertainties when determining the transmission efficiency of the metalenses. To overcome this situation, integral equation methods (IEMs) can be employed, as they compute the energy flow as a whole or as a collection of punctual sources with complex geometries.[24,25]

Based on the integral equation method,[26–29] in this contribution, we present the design of large DOF plasmonic metalenses consisting of arrays of nanoslits in a thin metallic layer. The width and position of the nanoslits were computed to match the phase of a Fresnel biprism (FB), an amplitude division interferometer widely used in optical systems to produce elongated cylindrical light beams. By using a home-made IEM program, we perform a numerical study of different parameters involved in the design of the PM, considering an incident Gaussian beam (GB), with the generation of focused wavefronts being demonstrated with DOF values of up to 150λ, contributing to the design of simplistic PMs for light focusing and imaging applications. The data that support the findings in this study are available from the corresponding author upon reasonable request.

II. DESIGN OF THE METALENSES

The departing point for the PM design is to consider the characteristics of a Fresnel biprism. This optical element divides an incident wavefront in two portions that interferes to produce a large waist reduced beam. The performance of the FB is ruled by its refractive index, n, and fabrication angle, α, formed by the base and each face of the prism [Fig. 1(a)]. The components of the wavevectors of the outcoming wavefronts from the prism can be geometrically determined, forming an angle $\gamma = \alpha(n-1)$ with respect to the z propagation axis. Hence, the phase is described by the relationship

$$\varphi_{FB} = kx \sin\gamma \pm 2m\pi, \tag{1}$$

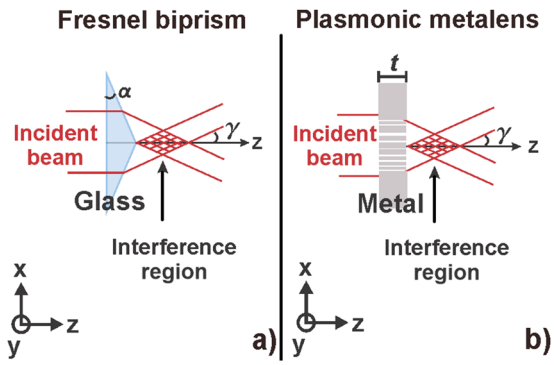

FIG. 1. Plasmonic metalens based on Fresnel's biprism. Schematic representation of (a) an incident beam at the base of a Fresnel biprism. The outcoming wavefronts generate an interference region along the z propagation axis limited by the angle γ and the width of the incident light beam, and (b) a plasmonic metalens based on the operation principle of the Fresnel biprism.

with m being an integer number and $k = 2\pi/\lambda$, with λ being the wavelength of incident light. We can notice from Eq. (1) that the interference region grows as γ decreases. Hence, by matching the phase of the FB to the phase of light outcoming from the PM, we would be able to generate an elongated beam.

The PM under design consists of an array of metallic nanoslits of width, w, in a gold film of thickness t. The nanoslits are distributed

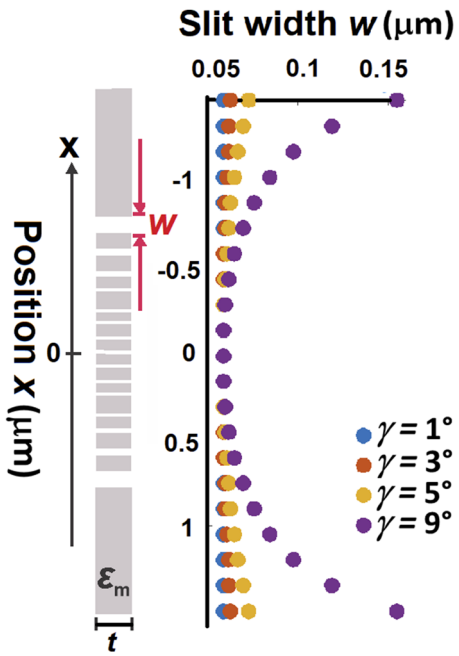

FIG. 2. Calculated distribution of the slit width to match the phase of a Fresnel biprism. Schematic of the nano-slits showing its opto-geometrical parameters, and width distribution of the gold nano-slits of thickness t = 300 nm. The incident light is a TM Gaussian beam at a wavelength of λ = 633 nm for $\gamma = [1, 3, 5, 9]°$.

along the x axis, and they are invariant along the y direction, following a cylindrical geometry [Fig. 1(b)]. Each nanoslit can be regarded as a metal–insulator–metal waveguide, whose transverse magnetic (TM) mode follows the dispersion relationship[16]

$$\tanh\left(\frac{w}{2}\sqrt{\beta^2 - k_0^2\varepsilon_d}\right) = -\frac{\varepsilon_d\sqrt{\beta^2 - k_0^2\varepsilon_m}}{\varepsilon_m\sqrt{\beta^2 - k_0^2\varepsilon_d}}, \tag{2}$$

where β and k_0 are the waveguide and free-space propagation constants, respectively, and ε_m and ε_d are the dielectric constants for the metal and the dielectric insulator, respectively. When light passes through the nanoslit, the outcoming wave will experience a phase shift given by $\varphi_{PM} = \beta t$, where t is the thickness of the metallic layer. Thus, by equating this phase shift to the phase of the FB, we can deduce the width of each nanoslit as a function of its position along the x axis measured from the center of the lens.

For instance, the plot in Fig. 2 shows the variation of the width for each nanoslit as a function of its position along the x axis for three different angles of the FB ($\gamma = [1, 3, 5, 9]^\circ$). In this plot, it is observed that the width of the nanoslits increases as they move away from the center when the values of the design angle γ increase. When γ is small, the PM will consist of a periodic array of nanoslits, in agreement with results reported in Ref. 22. For these results, we have considered an incident wavelength of λ = 633 nm, thickness of t = 300 nm for the gold layer, and air as the dielectric insulator (ε_d = 1.0), and the value for the dielectric constant of gold was taken from Ref. 30. Considering that the width of the nanoslits is smaller than the wavelength, we used the paraxial approximation for small angles when solving the dispersion relation.

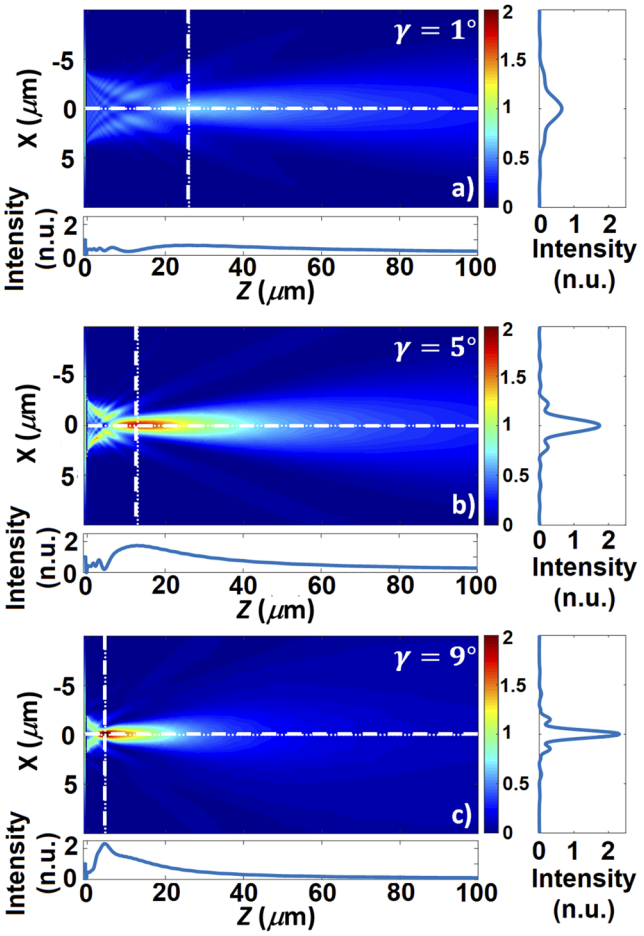

FIG. 3. Influence of γ in light focusing. Intensity maps of light at λ = 633 nm transmitted by the designed PM following the width distribution for the nano-slits of Fig. 2, for three different angles (a) γ = 1°, (b) γ = 5°, and (c) γ = 9°, and thickness t = 300 nm. The PSF and axial intensity profiles are plotted at the right and bottom of each map, respectively, taking the focal point (maximum intensity point) as a reference. The DOF increases when γ is reduced, while the intensity inversely increases.

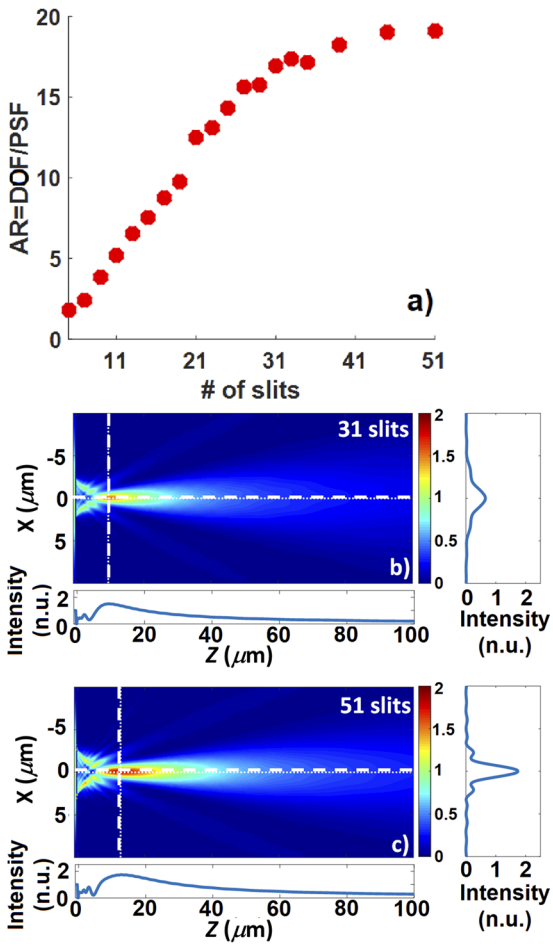

FIG. 4. Influence of the number of slits in light focusing. (a) Aspect ratio (*AR = DOF/PSF*) as a function of the number of slits. After 41 nano-slits, the aspect ratio tends to be a constant value. (b) and (c) Intensity maps, with PSF (right) and axial (bottom) intensity profiles, of the PM designed at λ = 633 nm and γ = 5° for 31 and 51 nanoslits, respectively. The transmitted light and directivity of the light beam increase with the number of slits.

III. NUMERICAL CHARACTERIZATION OF THE METALENSES

To numerically characterize the performance of the designed PM, we developed a homemade program based on the 2D integral equation method.[31] This is a rigorous method that solves the Maxwell equations from Green's second integral theorem in the quasi-static regime, by replacing the profile of the metalens by a collection of punctual light sources derived from the interaction between them and the incident Gaussian beam (GB).[26–29] With this method, it is possible to generate the electromagnetic field distribution and fully determine the transmission efficiency of the system in terms of the angular spectrum. The script was developed by following Refs. 27 and 29. Due to the invariant geometry of our metalenses along the y direction, in all our calculations, we used TM polarization defined by the field components $\vec{F} = (E_x, H_y, E_z)$ to satisfy the conditions for light propagation through the nanoslits.[16,17]

First, we analyzed the behavior of the PM for three different design angles: $\gamma = 1°$, $5°$, and $9°$. The design wavelength was $\lambda = 633$ nm, and we used 51 nanoslits for the PM. The results are shown in the intensity maps of Fig. 3, which are traced at the right side and below each map, the point spread function (PSF) and axial intensity, respectively, taking the position of the focal point as reference lines, defined as the point of maximum intensity.

As expected for a FB, from the maps in Fig. 3, it is observed that the DOF decreases when γ increases.[32] The transmission efficiency (measured in the far-field in terms of the angular spectrum and normalized to the power of the incident GB[29]) is around 20% for each PM. Hence, the PM with a shorter DOF achieves the maximum intensity concentration at the focal point, reaching the maximum intensity for the PM of $\gamma = 9°$ of 2.2 times, with respect to the

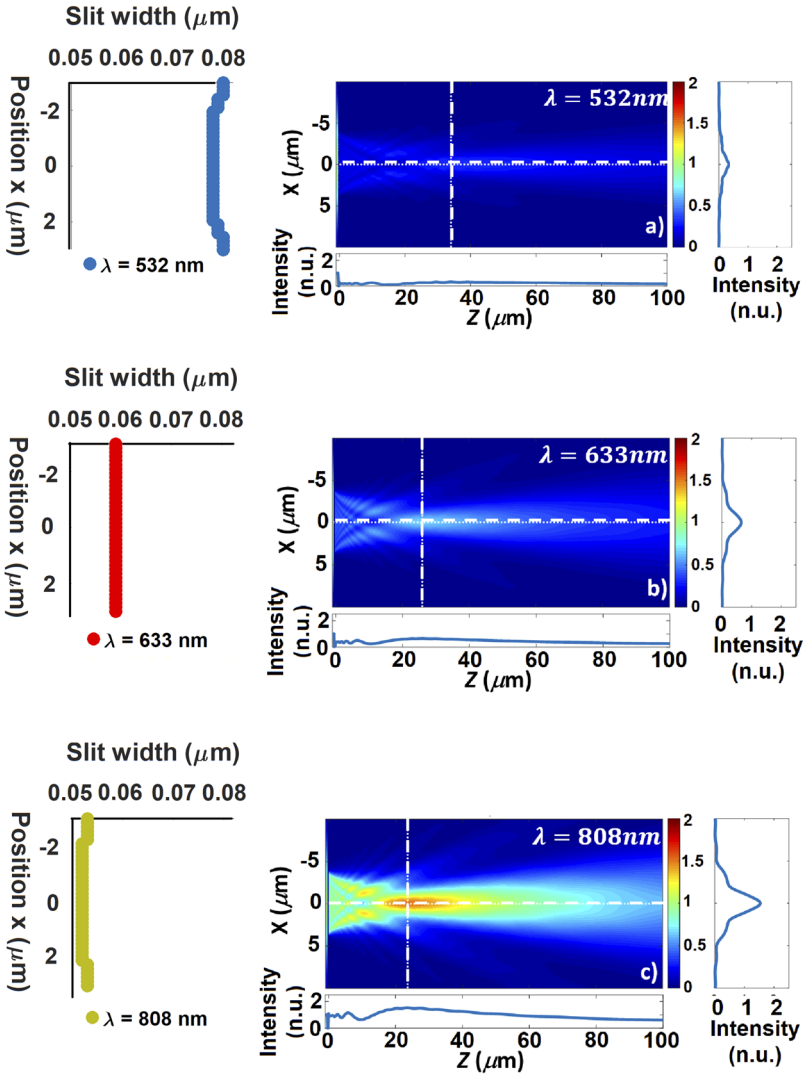

FIG. 5. Chromatic dependence on the design of plasmonic metalenses. Variation of w (left), intensity maps, and intensity profiles of large-DOF metalenses designed for three different wavelengths: (a) $\lambda = 532$ nm, (b) $\lambda = 633$ nm, and (c) $\lambda = 808$ nm. The design parameters were $t = 300$ nm, and $\gamma = 1°$ and 51 nano-slits. The DOF increases when the wavelength is reduced, while the transmission inversely drops.

incident beam. We must notice that the illumination of the system with a GB prevents the formation of the interference pattern expected for a FB.[33,34]

To determine the DOF and width of the PSF, we considered the distance from the focal point to the position where the intensity profiles drop to half of its maximum value along z and x axes. The DOF values are 80.31μm = 126.87λ, 29.09μm = 45.89λ, and 15.01μm = 23.71λ, while the PSF diameters are 2.88μm, 1.52μm, and 0.88μm, for $\gamma = 1°$, 5° and 9°, respectively.

Intuitively, the number of slits plays a role in the definition of the transmitted light beam. To understand this behavior, we computed the aspect ratio (AR) between the DOF and the PSF as a function of the number of slits, considering the same design parameters for the PM of Fig. 3(b) (λ = 633 nm, γ = 5°, and t = 300 nm). The plot in Fig. 4(a) summarizes the obtained results, with a linear growth of the AR value being observed, and after 41 slits, it remains almost unchanged. Figures 4(b) and 4(c) correspond to the intensity maps of this PM for 31 and 51 nanoslits. From these maps, it is observed that the intensity and position of the focal point increase with the number of slits. Consequently, increasing the number of nanoslits will result in a more directive beam with a longer DOF, as also reported in Ref. 22.

An important characteristic in the design of the metalenses is their chromatic dependence.[35,36] For this purpose, we designed three different PMs for three wavelengths of commonly used laser emission lines: λ = 532 nm, 633 nm, and 808 nm. For these PMs, we considered a design angle γ = 1°, thickness of the metallic layer t = 300 nm, and a fixed number of 51 nanoslits separated by a center to center distance of 150 nm. Figure 5 shows the obtained results for this analysis, where the plots in the left side of the intensity maps show the dependence of the width as a function of their axial distribution. For λ = 532 nm [Fig. 5(a)], the width of the nanoslits varies from 71 nm to 81 nm, with a light transmission of about 10%, intensity at the focal point of 0.33 times with respect to the incident GB, and a DOF of 81.19μm = 152.61λ. For the PM designed at λ = 633 nm [Fig. 5(b)], w remains in an almost constant value of 59 nm, transmission of 20%, intensity at the focal point of 0.65 times with respect to the incident GB, and DOF of 80.31μm = 126.87λ. For λ = 808 nm [Fig. 5(c)], w varies from 52 nm to 54 nm, transmission of 50%, intensity at the focal point of 1.54 times with respect to the incident GB, and a DOF of 63.83μm = 78.99λ. From these results, we can notice that the width of the nanoslits is larger for shorter wavelengths. Also, the DOF increases when the design wavelength is reduced, at the expense of reducing light transmission.

To complete the chromatic analysis, we illuminated the PM of Fig. 3(b) (γ = 5°, λ = 633 nm, t = 300 nm, and 51 nanoslits) with the same three different wavelengths (532 nm, 633 nm, and 808 nm). The resulting intensity maps are depicted in Fig. 6. For an incident wavelength of λ = 532 nm, the DOF is 27.60μm = 51.87λ with a transmission of 15%; for λ = 633 nm, the DOF is 29.05μm = 45.89λ with a transmission of 23%, and for λ = 808 nm, the DOF is 36.90μm = 45.66λ with a transmission of 44%. From these results, it is observed that when the wavelength is increased, the transmission efficiency increases, the focal point approaches the surface of the PM and the DOF is reduced. An interesting result is that the aspect ratio between DOF and PSF has a constant value of 20 for the three different illumination wavelengths.

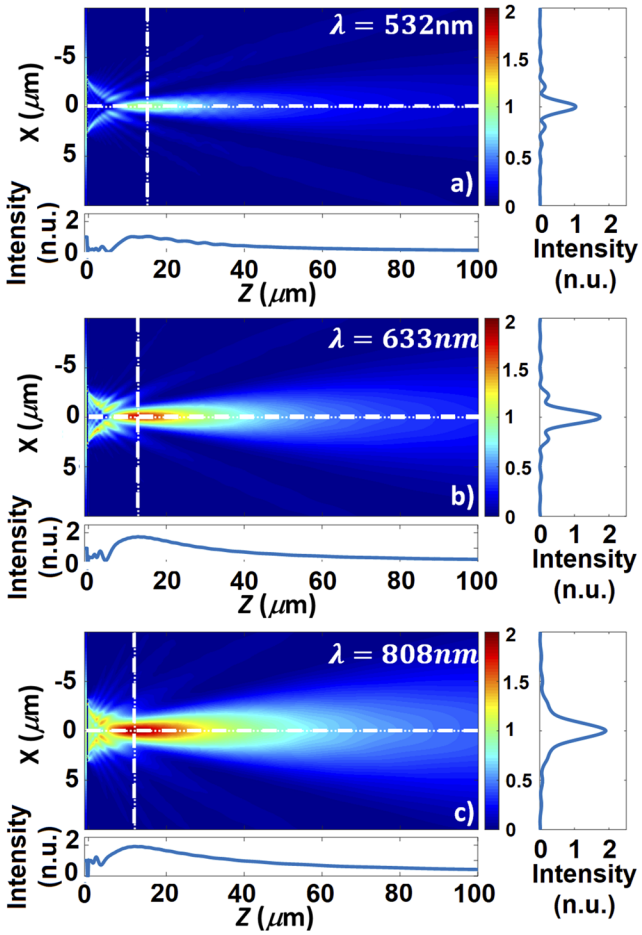

FIG. 6. Chromatic dependence of the plasmonic metalens. Intensity maps with their corresponding transverse (right) and axial (bottom) profiles for a PM designed for λ = 633 nm (γ = 5°, t = 300 nm, and 51 nano-slits) illuminated with three different wavelengths in the incident GB: (a) λ = 532 nm, (b) λ = 633 nm, and (c) λ = 808 nm. The DOF increases when the incidence wavelength is reduced, but the transmission efficiency inversely drops.

IV. CONCLUSIONS

By matching the phase of the wavefronts outcoming from a set of metallic nanoslits to the phase of the wavefronts outcoming from a Fresnel biprism, we were able to define the parameters for the design of large DOF plasmonic metalenses. By means of the integral equation method and in accordance with the bulk-optical system, we observed that by decreasing the design angle γ (propagation angle of the plane wavefronts outcoming from the FB), the DOF is increased. Also, as expected for a nanoslit metalens, the DOF and PSF increase with the number of slits made in the metallic film.

Based on our numerical results, we were able to design plasmonic metalenses with DOF values of up to 150λ for λ = 532 nm and transmission efficiencies of 50% for λ = 808 nm. We demonstrated that the aspect ratio between the DOF and the PSF reaches a constant value for a large number of nanoslits. Also, the metalenses

presented chromatic dependence but, interestingly, the aspect ratio remained constant when different illumination wavelengths were employed.

These results contribute to the design of simplistic metalenses that can be applied in small optical systems for imaging, focusing, and even communication applications.

ACKNOWLEDGMENTS

The authors thank CONACYT for partial financial support (Basic Scientific Research, Grant No. A1-S-21527). Adriana Inclán-Ladino thanks CONACYT for scholarship support.

REFERENCES

[1]T. W. Ebbesen, H. J. Lezec, H. F. Ghaemi, T. Thio, and P. A. Wolff, "Extraordinary optical transmission through sub-wavelength hole arrays," Nature **391**, 667 (1998).
[2]M. Khorasaninejad, W. T. Chen, R. C. Devlin, J. Oh, A. Y. Zhu, and F. Capasso, "Metalenses at visible wavelengths: Diffraction-limited focusing and subwavelength resolution imaging," Science **352**, 1190–1194 (2016).
[3]P. Lalanne and P. Chavel, "Metalenses at visible wavelengths: Past, present, perspectives," Laser Photonics Rev. **11**, 1600295 (2017).
[4]F. Aieta, M. A. Kats, P. Genevet, and F. Capasso, "Multiwavelength achromatic metasurfaces by dispersive phase compensation," Science **347**, 1342–1345 (2015).
[5]W. Song, S. Zheng, Y. Fu, C. Min, Y. Zhang, Z. Xie, and X. Yuan, "Control amplitude and phase of light by plasmonic meta-hologram with t-shaped nano-cavity," Chin. Opt. Lett. **17**, 062402 (2019).
[6]N. Yu, P. Genevet, M. A. Kats, F. Aieta, J.-P. Tetienne, F. Capasso, and Z. Gaburro, "Light propagation with phase discontinuities: Generalized laws of reflection and refraction," Science **334**, 333–337 (2011).
[7]Y. Zhang, X. Yang, and J. Gao, "Orbital angular momentum transformation of optical vortex with aluminum metasurfaces," Sci. Rep. **9**, 9133 (2019).
[8]D. Choi, Y. Lim, I.-M. Lee, S. Roh, and B. Lee, "Airy beam excitation using a subwavelength metallic slit array," IEEE Photonics Technol. Lett. **24**, 1440–1442 (2012).
[9]N. M. Litchinitser, "Structured light meets structured matter," Science **337**, 1054–1055 (2012), https://science.sciencemag.org/content/337/6098/1054.full.pdf.
[10]Y. Yuan, J. Niu, X. Ding, K. Zhang, and Q. Wu, "Planar metasurface as generator of bessel beam carrying orbital angular momentum," in *2016 International Symposium on Antennas and Propagation (ISAP)* (IEEE, 2016), pp. 188–189.
[11]M. Khorasaninejad and F. Capasso, "Metalenses: Versatile multifunctional photonic components," Science **358**, eaam8100 (2017).
[12]Z. Sun and H. K. Kim, "Refractive transmission of light and beam shaping with metallic nano-optic lenses," Appl. Phys. Lett. **85**, 642–644 (2004).
[13]F. M. Huang, N. Zheludev, Y. Chen, and F. Javier Garcia de Abajo, "Focusing of light by a nanohole array," Appl. Phys. Lett. **90**, 091119 (2007).
[14]X. M. Goh, L. Lin, and A. Roberts, "Plasmonic lenses for wavefront control applications using two-dimensional nanometric cross-shaped aperture arrays," J. Opt. Soc. Am. B **28**, 547–553 (2011).
[15]C. E. Garcia-Ortiz, R. Cortes, J. E. Gómez-Correa, E. Pisano, J. Fiutowski, D. A. Garcia-Ortiz, V. Ruiz-Cortes, H.-G. Rubahn, and V. Coello, "Plasmonic metasurface luneburg lens," Photonics Res. **7**, 1112–1118 (2019).
[16]H. Shi, C. Wang, C. Du, X. Luo, X. Dong, and H. Gao, "Beam manipulating by metallic nano-slits with variant widths," Opt. Express **13**, 6815–6820 (2005).
[17]L. Verslegers, P. B. Catrysse, Z. Yu, J. S. White, E. S. Barnard, M. L. Brongersma, and S. Fan, "Planar lenses based on nanoscale slit arrays in a metallic film," Nano Lett. **9**, 235–238 (2008).
[18]E. Bayati, R. Pestourie, S. Colburn, Z. Lin, S. G. Johnson, and A. Majumdar, "Inverse designed metalenses with extended depth of focus," ACS Photonics (published online).
[19]M. Veysi, C. Guclu, O. Boyraz, and F. Capolino, "Reflective metasurface lens with an elongated needle-shaped focus," J. Opt. Soc. Am. B **34**, 374–382 (2017).
[20]Z. Zhang, D. Wen, C. Zhang, M. Chen, W. Wang, S. Chen, and X. Chen, "Multifunctional light sword metasurface lens," ACS Photonics **5**, 1794–1799 (2018).
[21]J. Guan, J. Lin, C. Chen, Y. Ma, J. Tan, and P. Jin, "Transversely polarized sub-diffraction optical needle with ultra-long depth of focus," Opt. Commun. **404**, 118–123 (2017).
[22]L. Cheng, P. Cao, Y. Li, W. Kong, X. Zhao, and X. Zhang, "High efficient far-field nanofocusing with tunable focus under radial polarization illumination," Plasmonics **7**, 175–184 (2012).
[23]H. J. Lezec, A. Degiron, E. Devaux, R. A. Linke, L. Martin-Moreno, F. J. Garcia-Vidal, and T. W. Ebbesen, "Beaming light from a subwavelength aperture," Science **297**, 820–822 (2002), https://science.sciencemag.org/content/297/5582/820.full.pdf.
[24]A. M. Kern and O. J. F. Martin, "Surface integral formulation for 3D simulations of plasmonic and high permittivity nanostructures," J. Opt. Soc. Am. A **26**, 732–740 (2009).
[25]C. Warren, S. Sesnic, A. Ventura, L. Pajewski, D. Poljak, and A. Giannopoulos, "Comparison of time-domain finite-difference, finite-integration, and integral-equation methods for dipole radiation in half-space environments," Prog. Electromagn. Res. M **57**, 175–183 (2017).
[26]A. A. Maradudin, E. R. Méndez, and T. Michel, "Backscattering effects in the elastic scattering of p-polarized light from a large-amplitude random metallic grating," Opt. Lett. **14**, 151–153 (1989).
[27]A. A. Maradudin, T. Michel, A. R. McGurn, and E. R. Méndez, "Enhanced backscattering of light from a random grating," Ann. Phys. **203**, 255–307 (1990).
[28]Z.-H. Gu, R. S. Dummer, A. A. Maradudin, A. R. McGurn, and E. R. Mendez, "Enhanced transmission through rough-metal surfaces," Appl. Opt. **30**, 4094–4102 (1991).
[29]C. I. Valencia, E. R. Méndez, and B. S. Mendoza, "Second-harmonic generation in the scattering of light by an infinite cylinder," J. Opt. Soc. Am. B **21**, 36–44 (2004).
[30]P. B. Johnson and R. W. Christy, "Optical constants of the noble metals," Phys. Rev. B **6**, 4370 (1972).
[31]R. Tellez-Limon, "Lentes de nano-rendijas (Nano-slit lenses)," M.S. thesis, CICESE, 2011.
[32]E. Hecht, *Optics* (Pearson education, Addison-Wesley, 2002).
[33]O. Brzobohatý, T. Cižmár, and P. Zemánek, "High quality quasi-bessel beam generated by round-tip axicon," Opt. Express **16**, 12688–12700 (2008).
[34]M. Anguiano-Morales, A. Martínez, M. D. Iturbe-Castillo, and S. Chávez-Cerda, "Different field distributions obtained with an axicon and an amplitude mask," Opt. Commun. **281**, 401–407 (2008).
[35]S. Wang, P. C. Wu, V.-C. Su, Y.-C. Lai, M.-K. Chen, H. Y. Kuo, B. H. Chen, Y. H. Chen, T.-T. Huang, J.-H. Wang *et al.*, "A broadband achromatic metalens in the visible," Nat. Nanotechnol. **13**, 227 (2018).
[36]S. Shrestha, A. C. Overvig, M. Lu, A. Stein, and N. Yu, "Broadband achromatic dielectric metalenses," Light: Sci. Appl. **7**, 85 (2018).